FDTD Analysis of Lossy, Multiconductor Transmission Lines Terminated in Arbitrary Loads

Antonio Orlandi, *Member, IEEE,* and Clayton R. Paul, *Fellow, IEEE*

Abstract— **A hybrid method is presented for incorporating general terminations into the solution of lossy multiconductor transmission lines (MTL's). The terminations are characterized by a state-variable formulation which allows a general characterization of dynamic as well as nonlinear elements in the termination networks. The method combines the second-order accuracy of the finite difference-time domain (FDTD) algorithm for the MTL with the absolutely stable, backward Euler discretization of the state-variable representations of the termination networks. A compact matrix formulation of the recursion relations at the interface between the MTL and the termination networks allows a straightforward coding of the algorithm. Skin effect losses of the line conductors as well as the effect of an incident field are easily incorporated into the algorithm. Several numerical examples are given which contain dynamic and nonlinear elements in the terminations. These examples demonstrate the validity of the method and show that the temporal and spatial step sizes can be maximized, thereby minimizing the computational burden.**

I. Introduction

THE increasing demand for higher speeds of data processing in information processing systems has caused a renewed interest in modeling various nonideal effects of the conductors that interconnect the various subsystems. The increasing speeds are accompanied by a corresponding decrease in pulse rise/fall times. This accentuates the high-frequency spectral content of those signals and causes the skin effect loss in the conductors to take on increasing importance. This skin effect loss depends on the square root of frequency making its direct incorporation into time-domain analysis difficult. The method to be presented easily incorporates this skin effect loss into the time-domain solution. Because of the increasing density of components, crosstalk, as well as the effects of incident fields, also take on increasing importance in these systems.

Perhaps the most direct and computationally efficient model of these interconnect lines is through the multiconductor transmission line (MTL) equations [1]. Digital systems contain nonlinear loads which generally requires the direct, time-domain solution of the MTL equations. There are efficient, indirect methods of obtaining the time-domain solution in which the skin effect losses can be readily incorporated. One such indirect method is the time-domain to frequency-domain (TDFD) transformation, wherein the time-domain response is obtained from the frequency response via the Fourier transformation [1]. Frequency-dependent losses can be readily handled in computing the frequency-domain transfer function. However, this method inherently relies on superposition which is invalid for nonlinear terminations. Other similar methods which employ frequency domain data may or may not be valid for the same reason, depending on whether they include the nonlinear terminations in the transfer function, thereby making the system nonlinear, or only characterize the linear line as a multiport [1]. The finite-difference time-domain (FDTD) method is a general way of directly obtaining the time-domain response [1], [2]. The MTL equations are discretized in position along the line and in time, and the resulting difference equations are solved in a leapfrog fashion. There are no inherent restrictions on the nature of the terminations with this model. However, the implementation depends on the type of termination. The predominant type of termination in the FDTD analysis is resistive [1], [3], [4]. A recent result characterizes the terminations using the modified nodal analysis (MNA) formulation which allows for more general terminations [5]. In this paper, we will characterize the transmission line using the FDTD method, and the termination networks will be characterized using the state-variable formulation [10], [11]. The state-variable characterization of the terminations also allows the consideration of general termination networks and is simpler to interface with the FDTD formulation. This also allows a straightforward coding of the resulting algorithm.

We will briefly discuss the FDTD algorithm for a typical line in Section II. A novel way of generating the link between the variables in the FDTD model of the line and the variables in the termination networks at its endpoints will be given. Interfacing the FDTD model of the line with the state-variable description will be demonstrated in Section III. A compact matrix result for the recursion relations will be given. The adaptation of the model to nonlinear terminations will be given in Section IV. Computed results for dynamic terminations using this new formulation will be given in Section V and will be compared to the predictions from various other models in order to demonstrate the validity of the method.

II. The FDTD Recursion Relations

Consider a $(n+1)$ conductor, uniform transmission line shown in Fig. 1. The MTL equations for the general case of imperfect conductors immersed in an incident field are [1]

$$\frac{\partial}{\partial z}\mathbf{V}(z,t)+\mathbf{Z}_i(t)*\mathbf{I}(z,t)+\mathbf{L}\frac{\partial}{\partial t}\mathbf{I}(z,t)=-\frac{\partial}{\partial z}\mathbf{E}_T(z,t)+\mathbf{E}_L(z,t) \tag{1a}$$

Manuscript received November 6, 1995; revised April 26, 1996.

A. Orlandi is with the Department of Electrical Engineering, University of L'Aquila, Italy.

C. R. Paul is with the Department of Electrical Engineering, University of Kentucky, Lexington, KY 40506 USA.

Publisher Item Identifier S 0018-9375(96)06143-1.

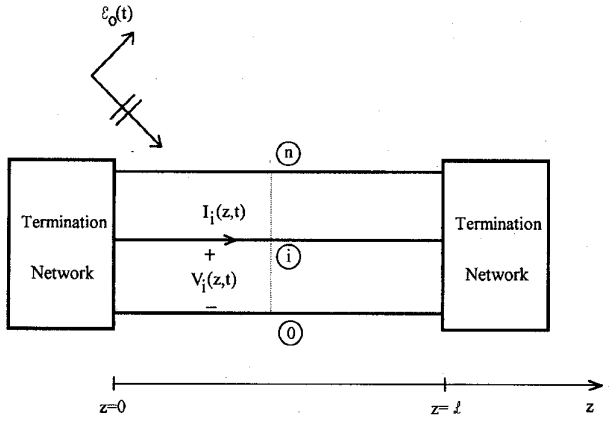

Fig. 1. Illustration of a general multiconductor transmission line (MTL).

$$\frac{\partial}{\partial z}\mathbf{I}(z,\,t)+\mathbf{C}\frac{\partial}{\partial t}\mathbf{V}(z,\,t)=-\mathbf{C}\frac{\partial}{\partial t}\mathbf{E}_T(z,\,t) \tag{1b}$$

where $\mathbf{V}$ and $\mathbf{I}$ are $n\times 1$ vectors of the line voltages (with respect to the reference conductor) and line currents, respectively. The position along the line is denoted as z. The line voltages and currents are functions of z and time t. Convolution in the time domain is denoted by $*$. The line cross-sectional dimensions are contained in the per-unit-length parameter matrices $\mathbf{L}$ (inductance) and $\mathbf{C}$ (capacitance). The conductor losses are represented by $\mathbf{Z}_i(t)$ which is the inverse Laplace transform of

$$\mathbf{Z}_i(t)\Leftrightarrow\mathbf{Z}_i(s)=\mathbf{R}(s)+s\mathbf{L}_i(s). \tag{2}$$

where s is the Laplace transformation variable. This conductor internal impedance contains both resistance, $\mathbf{R}$, and internal inductance (due to the magnetic flux internal to the conductors), $\mathbf{L}_i$. At low frequencies the current is uniformly distributed over the conductor cross section. This gives rise to a dc per-unit-length resistance, $r_{\rm dc}$, and a portion of the per-unit-length inductance due to magnetic flux internal to the conductor, $l_{i,\,\rm dc}$. At the higher frequencies, the current flows near the conductor surface and asymptotically approaches a distribution equivalent to the current being uniformly distributed over a region at the conductor surface of thickness equal to a skin depth, $\delta=1/\sqrt{\pi f\mu\sigma}$. Thus, the high-frequency resistance increases as $\sqrt{f}$ and the internal inductance decreases as $\sqrt{f}$.

The quantities $\mathbf{E}_T(z,\,t)$ and $\mathbf{E}_L(z,\,t)$ are $n\times 1$ vectors containing the components of the incident electric field that are transverse to the line and parallel to the line conductors, respectively, with the line conductors removed [1]. The quantity $[\mathbf{E}_T(z,\,t)]_i$

$$[\mathbf{E}_T(z,\,t)]_i=\int_{c_i}\mathcal{E}^{\rm incident}\cdot d\vec{l} \tag{3}$$

is the integral of the component of the incident electric field intensity vector that is in a plane transverse to the line conductors. Contour c_i lies in this transverse plane and is between the reference conductor and the ith conductor. The quantity $[\mathbf{E}_L(z,\,t)]_i$ is the difference between the longitudinal (z directed) components of the incident electric field intensity vector along the position of the ith conductor and along the position of the reference conductor (with those conductors absent):

$$[\mathbf{E}_L(z,\,t)]_i=\mathcal{E}_z^{\rm incident}(i\text{th conductor},\,z,\,t)-\mathcal{E}_z^{\rm incident}(\text{reference conductor},\,z,\,t). \tag{4}$$

A common way of representing the skin effect losses of the conductors is [6]

$$\mathbf{Z}_i(s)=\mathbf{A}+\mathbf{B}\sqrt{s}. \tag{5}$$

The corresponding frequency-domain result is obtained by substituting $s\Leftrightarrow j\omega$ giving

$$\mathbf{Z}_i(\omega)=\mathbf{A}+\mathbf{B}\sqrt{j\omega}=\mathbf{A}+\mathbf{B}\sqrt{\pi}\sqrt{f}\,(1+j). \tag{6}$$

Thus, we may interpret, in this approximation,

$$\mathbf{A}=\mathbf{R}_{\rm dc} \tag{7a}$$

$$\mathbf{B}\sqrt{\pi}\sqrt{f}=\mathbf{R}_{hf} \tag{7b}$$

$$\mathbf{L}_{i,\,hf}=\frac{1}{2\sqrt{\pi}\sqrt{f}}\mathbf{B}. \tag{7c}$$

The approximation of the conductor internal impedance given in (5) provides for a simple time-domain result. This is due to the fact that the reciprocal of $\sqrt{s}$ has a simple inverse transform in the time domain which is [2], [7], [8]

$$\frac{1}{\sqrt{s}}\Leftrightarrow\frac{1}{\sqrt{\pi}}\frac{1}{\sqrt{t}}. \tag{8}$$

The product of the internal impedance and the current in the MTL equations translates, in the time domain, to a convolution as

$$\mathbf{Z}_i(s)\mathbf{I}(z,\,s)\Leftrightarrow\mathbf{Z}_i(t)*\mathbf{I}(z,\,t). \tag{9}$$

Substituting the approximation in (5) gives

$$\mathbf{Z}_i(s)\mathbf{I}(z,\,s)=\mathbf{A}\mathbf{I}(z,\,s)+\mathbf{B}\left[\frac{1}{\sqrt{s}}\right]s\mathbf{I}(z,\,s)$$

$$\Updownarrow$$

$$\mathbf{Z}_i(t)*\mathbf{I}(z,\,t)=\mathbf{A}\mathbf{I}(z,\,t)+\frac{1}{\sqrt{\pi}}\mathbf{B}\cdot\left[\int_0^t\frac{1}{\sqrt{\tau}}\frac{\partial}{\partial(t-\tau)}\mathbf{I}(z,\,t-\tau)\,d\tau\right]. \tag{10}$$

In order to discretize these transmission-line equations, we divide the line axis into NDZ sections each of length Δz as shown in Fig. 2(b). Similarly, we divide the total solution time into NDT segments of length Δt. To provide second-order accuracy of the discretization we interlace the NDZ + 1 voltage points, $V_1,\,V_2,\,\cdots,\,V_{\rm NDZ},\,V_{\rm NDZ+1}$, and the NDZ current points, $I_1,\,I_2,\,\cdots,\,I_{\rm NDZ}$ as shown in [9, Fig. 2(a)]. Each voltage and adjacent current solution point is separated by $\Delta z/2$. In addition, the time points are also interlaced, and each voltage time point and adjacent current time point are separated by $\Delta t/2$ [9]. The convolution in (10) is approximated in the following manner where the function $\mathbf{F}(t)$ (which represents the derivative of the line current in the MTL equations) is approximated as constant over the Δt

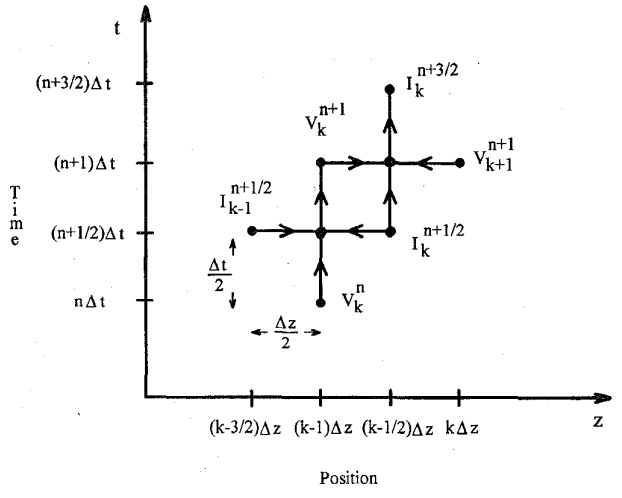

(a)

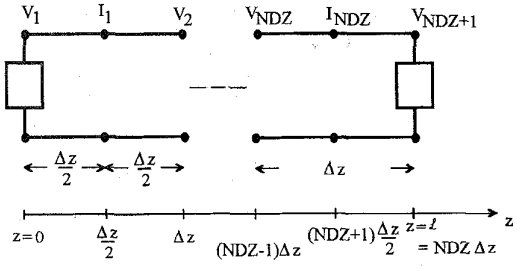

(b)

Fig. 2. Illustration of (a) the FDTD discretization of the voltages and currents along the MTL and (b) the locations of the solution variables on the line.

segments [1], [2]:

$$\int_0^t \frac{1}{\sqrt{\tau}}\,\mathbf{F}(t-\tau)\,d\tau \cong \int_0^{(n+1)\Delta t} \frac{1}{\sqrt{\tau}}\,\mathbf{F}[(n+1)\Delta t-\tau]\,d\tau \cong \sum_{m=0}^{n} \mathbf{F}^{n+1-m} \int_{m\Delta t}^{(m+1)\Delta t} \frac{1}{\sqrt{\tau}}\,d\tau = \sqrt{\Delta t}\sum_{m=0}^{n} \mathbf{F}^{n+1-m}\,Z_0(m) \tag{11}$$

where

$$Z_0(m) = \int_m^{(m+1)} \frac{1}{\sqrt{\varsigma}}\,d\varsigma. \tag{12}$$

Discretizing the derivatives in the MTL equations using second-order central differences according to the scheme in Fig. 2(a) and substituting (11) gives

$$\frac{1}{\Delta z}[\mathbf{V}_{k+1}^{n+1}-\mathbf{V}_k^{n+1}] + \frac{1}{\Delta t}\mathbf{L}[\mathbf{I}_k^{n+3/2}-\mathbf{I}_k^{n+1/2}] + \tfrac{1}{2}\mathbf{A}[\mathbf{I}_k^{n+3/2}+\mathbf{I}_k^{n+1/2}] + \frac{1}{\sqrt{\pi}\sqrt{\Delta t}}\cdot\mathbf{B}\sum_{m=0}^{n} Z_0(m)[\mathbf{I}_k^{n+3/2-m}-\mathbf{I}_k^{n+1/2-m}] = -\frac{1}{\Delta z}[\mathbf{E}_{T,k+1}^{n+1}-\mathbf{E}_{T,k}^{n+1}] + \frac{1}{2}[\mathbf{E}_{L,k}^{n+3/2}+\mathbf{E}_{L,k}^{n+1/2}] \quad k=1,2,\cdots,\mathrm{NDZ} \tag{13a}$$

$$\frac{1}{\Delta z}[\mathbf{I}_k^{n+1/2}-\mathbf{I}_{k-1}^{n+1/2}] + \frac{1}{\Delta t}\mathbf{C}[\mathbf{V}_k^{n+1}-\mathbf{V}_k^n] = -\frac{1}{\Delta t}\mathbf{C}[\mathbf{E}_{T,k}^{n+1}-\mathbf{E}_{T,k}^n] \quad k=2,\cdots,\mathrm{NDZ} \tag{13b}$$

where we denote

$$\mathbf{V}_k^n \equiv \mathbf{V}\,[(k-1)\Delta z,\, n\Delta t] \tag{14a}$$

$$\mathbf{I}_k^n \equiv \mathbf{I}\,[(k-\tfrac{1}{2})\Delta z,\, n\Delta t]. \tag{14b}$$

The transverse incident field sources, $\mathbf{E}_T(z,t)$, are to be evaluated at the voltage positions, whereas the longitudinal field sources, $\mathbf{E}_L(z,t)$, are to be evaluated at the current positions, i.e.,

$$\mathbf{E}_{T,k}^n \equiv \mathbf{E}_T[(k-1)\,\Delta z,\, n\Delta t] \tag{15a}$$

$$\mathbf{E}_{L,k}^n \equiv \mathbf{E}_L[(k-\tfrac{1}{2})\,\Delta z,\, n\Delta t]. \tag{15b}$$

The required recursion relations for the interior points on the line are obtained by solving (13a) and (13b) giving

$$\left[\frac{\Delta z}{\Delta t}\mathbf{L}+\frac{\Delta z}{2}\mathbf{A}+\frac{\Delta z}{\sqrt{\pi\Delta t}}Z_0(0)\mathbf{B}\right]\mathbf{I}_k^{n+3/2} = \left[\frac{\Delta z}{\Delta t}\mathbf{L}-\frac{\Delta z}{2}\mathbf{A}+\frac{\Delta z}{\sqrt{\pi\Delta t}}Z_0(0)\mathbf{B}\right]\mathbf{I}_k^{n+1/2} - \frac{\Delta z}{\sqrt{\pi}\sqrt{\Delta t}}\mathbf{B}\sum_{m=1}^{n} Z_0(m)[\mathbf{I}_k^{n+3/2-m}-\mathbf{I}_k^{n+1/2-m}] - (\mathbf{V}_{k+1}^{n+1}-\mathbf{V}_k^{n+1}) - [\mathbf{E}_{T,k+1}^{n+1}-\mathbf{E}_{T,k}^{n+1}] + \frac{\Delta z}{2}[\mathbf{E}_{L,k}^{n+3/2}+\mathbf{E}_{L,k}^{n+1/2}] \tag{16a}$$

$$\mathbf{V}_k^{n+1} = \mathbf{V}_k^n - \frac{\Delta t}{\Delta z}\mathbf{C}^{-1}(\mathbf{I}_k^{n+1/2}-\mathbf{I}_{k-1}^{n+1/2}) - [\mathbf{E}_{T,k}^{n+1}-\mathbf{E}_{T,k}^n]. \tag{16b}$$

Equations (16a) and (16b) are solved in a leap frog fashion. First the voltages along the line are obtained, for a fixed time, from (16b) in terms of the previous solutions. Then the currents are obtained from (16a) in terms of the voltages from (16b) as well as previously obtained values. The solution starts with an initially-relaxed line having zero voltage and current values.

Next, consider the incorporation of the terminal conditions. The essential problem in incorporating the terminal conditions is that the FDTD voltages and currents at each end of the line, $\mathbf{V}_1$, $\mathbf{I}_1$, and $\mathbf{V}_{NDZ+1}$, $\mathbf{I}_{NDZ}$, are not collocated in space or time, whereas the terminal conditions relate the voltage and current at the same position and at the same time. We will denote the vector of currents at the source ($z=0$) as $\mathbf{I_S}$ and the vector of currents at the load ($z=\mathcal{L}$) as $\mathbf{I_L}$ as shown in Fig. 3. Observe that $\mathbf{I_L}$ is defined as being directed out of the termination network (into the line) as is $\mathbf{I_S}$. The second transmission-line equation given in (1b) is discretized at the source as

$$\frac{1}{\frac{\Delta z}{2}}\left[\mathbf{I}_1^{n+1/2}-\frac{\mathbf{I}_S^{n+1}+\mathbf{I}_S^n}{2}\right] + \frac{1}{\Delta t}\mathbf{C}[\mathbf{V}_1^{n+1}-\mathbf{V}_1^n] = -\frac{1}{\Delta t}\mathbf{C}[\mathbf{E}_{T,1}^{n+1}-\mathbf{E}_{T,1}^n]. \tag{17}$$

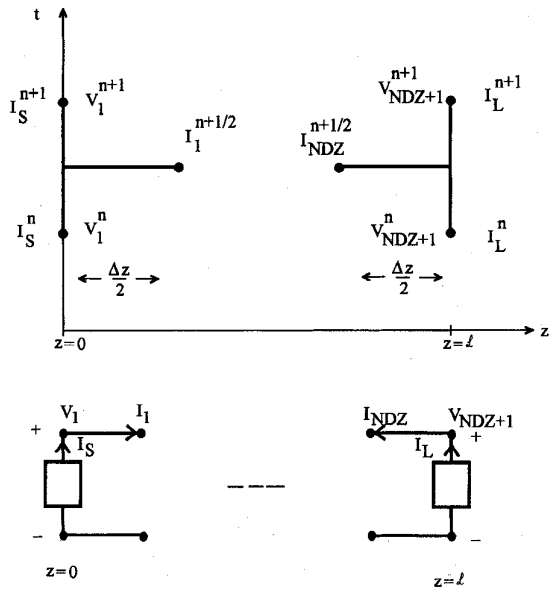

Fig. 3. Illustration of the FDTD discretization of the voltages and currents at the MTL terminations.

Similarly, the second transmission-line equation, (1b), is discretized at the load as

$$\frac{1}{\frac{\Delta z}{2}}\left[-\frac{\mathbf{I}_L^{n+1}+\mathbf{I}_L^n}{2}+\mathbf{I}_{\mathrm{NDZ}}^{n+1/2}\right] + \frac{1}{\Delta t}\mathbf{C}\left[\mathbf{V}_{\mathrm{NDZ}+1}^{n+1}-\mathbf{V}_{\mathrm{NDZ}+1}^n\right] = -\frac{1}{\Delta t}\mathbf{C}[\mathbf{E}_{T,\,\mathrm{NDZ}+1}^{n+1}-\mathbf{E}_{T,\,\mathrm{NDZ}+1}^n]. \tag{18}$$

Observe that the last current point on the line, $\mathbf{I}_{\mathrm{NDZ}}$, is directed into the line in order to provide symmetry of the following results. Equations (17) and (18) are solved to give the recursion relations at the source and the load

$$\mathbf{V}_1^{n+1} = \mathbf{V}_1^n - \frac{2\Delta t}{\Delta z}\mathbf{C}^{-1}\mathbf{I}_1^{n+1/2} + \frac{\Delta t}{\Delta z}\mathbf{C}^{-1}[\mathbf{I}_S^{n+1}+\mathbf{I}_S^n]-[\mathbf{E}_{T,1}^{n+1}-\mathbf{E}_{T,1}^n] \tag{19a}$$

$$\mathbf{V}_{\mathrm{NDZ}+1}^{n+1} = \mathbf{V}_{\mathrm{NDZ}+1}^n - \frac{2\Delta t}{\Delta z}\mathbf{C}^{-1}\mathbf{I}_{\mathrm{NDZ}}^{n+1/2} + \frac{\Delta t}{\Delta z}\mathbf{C}^{-1}[\mathbf{I}_L^{n+1}+\mathbf{I}_L^n] - [\mathbf{E}_{T,\,\mathrm{NDZ}+1}^{n+1}-\mathbf{E}_{T,\,\mathrm{NDZ}+1}^n]. \tag{19b}$$

It should be pointed out that the method of obtaining collocated current and voltage relations in (19) at the source and the load can be shown to yield the exact solution of a two-conductor line consisting of perfect conductors immersed in a lossless, homogeneous medium [1], [9]. In the multiconductor case consisting of imperfect conductors and/or inhomogeneous media, this has not been demonstrated. However, extensive computations by the authors for these cases have shown that the above technique yields very accurate results.

III. State-Variable Formulation of the Terminal Constraints

Any stable, lumped network can be completely characterized in a state-variable form [10], [11]. In the case of a linear network, this completely general formulation becomes

$$\frac{d}{dt}\mathbf{X}(t) = \mathbf{M}\mathbf{X}(t) + \mathbf{N}\mathbf{U}(t) \tag{20a}$$

with an associated output relation

$$\mathbf{Y}(t) = \mathbf{O}\mathbf{X}(t) + \mathbf{P}\mathbf{U}(t) + \mathbf{Q}\frac{d}{dt}\mathbf{U}(t). \tag{20b}$$

The vector $\mathbf{X}$ contains the state variables of the lumped network. These are typically the inductor currents and capacitor voltages in that network or some subset of those variables. The vector $\mathbf{U}$ contains the independent sources in the network (the inputs), and the vector $\mathbf{Y}$ contains the designated outputs (currents and/or voltages) of the network. It should be emphasized that this formulation can characterize general linear networks, which may contain such diverse conditions as inductor-current source cutsets and/or capacitor-voltage source loops, as well as controlled sources of all types.

Consider the recursion relations at the endpoints of the line given in (19a) and (19b). From these relations, it is clear that we must configure the state-variable representations of the termination networks such that the outputs are the currents $\mathbf{I}_S$ and $\mathbf{I}_L$. The inputs for the state-variable representations must be the line voltages at the endpoints, $\mathbf{V}_1$ and $\mathbf{V}_{\mathrm{NDZ}+1}$, as well as the independent sources, $\mathbf{S}_S$ and $\mathbf{S}_L$, within the termination networks. In order to accomplish this task we will define the outputs in (20) as $\mathbf{I}_S$ and $\mathbf{I}_L$ and will partition the input vectors to yield

$$\frac{d}{dt}\mathbf{X}_S(t) = \mathbf{M}_S\mathbf{X}_S(t) + \mathbf{N}_1\mathbf{V}_1(t) + \mathbf{N}_S\mathbf{S}_S(t) \tag{21a}$$

$$\mathbf{I}_S(t) = \mathbf{O}_S\mathbf{X}_S(t) + \mathbf{P}_1\mathbf{V}_1(t) + \mathbf{P}_S\mathbf{S}_S(t) + \mathbf{Q}_1\frac{d}{dt}\mathbf{V}_1(t) + \mathbf{Q}_S\frac{d}{dt}\mathbf{S}_S(t) \tag{21b}$$

$$\frac{d}{dt}\mathbf{X}_L(t) = \mathbf{M}_L\mathbf{X}_L(t) + \mathbf{N}_{\mathrm{NDZ}+1}\mathbf{V}_{\mathrm{NDZ}+1}(t) + \mathbf{N}_L\mathbf{S}_L(t) \tag{22a}$$

$$\mathbf{I}_L(t) = \mathbf{O}_L\mathbf{X}_L(t) + \mathbf{P}_{\mathrm{NDZ}+1}\mathbf{V}_{\mathrm{NDZ}+1}(t) + \mathbf{P}_L\mathbf{S}_L(t) + \mathbf{Q}_{\mathrm{NDZ}+1}\frac{d}{dt}\mathbf{V}_{\mathrm{NDZ}+1}(t) + \mathbf{Q}_L\frac{d}{dt}\mathbf{S}_L(t) \tag{22b}$$

where S and L refer to the networks at the source and load ends, respectively. Observe that in this state-variable characterization of the termination networks, the terminal voltages, $\mathbf{V}_1$ and $\mathbf{V}_{\mathrm{NDZ}+1}$, are treated as being independent voltage sources driving the terminations.

We now address the problem of interfacing the state-variable characterizations of the termination networks with the recursion relations for the attached line. We need to discretize the state-variable forms in (21) and (22). We will choose the implicit backward Euler method (also called the first-order Adams–Moulton algorithm) which is absolutely

stable regardless of time step size so long as the termination network itself is stable–a necessary assumption [10]. Because of this, the stability condition on Δt must be enforced only on the solution for the MTL portion of the system. The state-variable forms in (21) for the source termination network are discretized using the backward Euler method to yield [10]

$$\mathbf{X}_S^{n+1} = \mathbf{X}_S^n + \Delta t[\mathbf{M}_S\mathbf{X}_S^{n+1} + \mathbf{N}_1\mathbf{V}_1^{n+1} + \mathbf{N}_S\mathbf{S}_S^{n+1}] \quad (23a)$$

$$\begin{aligned}\mathbf{I}_S^{n+1} &= \mathbf{O}_S\mathbf{X}_S^{n+1} + \mathbf{P}_1\mathbf{V}_1^{n+1} + \mathbf{P}_S\mathbf{S}_S^{n+1} \\ &\quad + \frac{1}{\Delta t}\mathbf{Q}_1[\mathbf{V}_1^{n+1} - \mathbf{V}_1^n] \\ &\quad + \frac{1}{\Delta t}\mathbf{Q}_S[\mathbf{S}_S^{n+1} - \mathbf{S}_S^n].\end{aligned} \quad (23b)$$

Solving (23a) for $\mathbf{X}_S^{n+1}$ yields

$$\begin{aligned}[\mathbf{1}_n - \Delta t\mathbf{M}_S]\mathbf{X}_S^{n+1} &= \mathbf{X}_S^n + \Delta t\mathbf{N}_1\mathbf{V}_1^{n+1} \\ &\quad + \Delta t\mathbf{N}_S\mathbf{S}_S^{n+1} \quad (24a)\\ \mathbf{I}_S^{n+1} &= \mathbf{O}_S\mathbf{X}_S^{n+1} + \mathbf{P}_1\mathbf{V}_1^{n+1} + \mathbf{P}_S\mathbf{S}_S^{n+1} \\ &\quad + \frac{1}{\Delta t}\mathbf{Q}_1[\mathbf{V}_1^{n+1} - \mathbf{V}_1^n] \\ &\quad + \frac{1}{\Delta t}\mathbf{Q}_S[\mathbf{S}_S^{n+1} - \mathbf{S}_S^n] \quad (24b)\end{aligned}$$

where $\mathbf{1}_n$ is the $n \times n$ identity matrix with one's on the main diagonal and zero's elsewhere. Substituting (24b) into (19a) and combining with (24a) yields

$$\begin{aligned}&\begin{bmatrix}\left(\frac{\Delta z}{\Delta t}\mathbf{C} - \mathbf{P}_1 - \frac{1}{\Delta t}\mathbf{Q}_1\right) & -\mathbf{O}_S \\ -\Delta t\mathbf{N}_1 & \mathbf{1}_n - \Delta t\mathbf{M}_S\end{bmatrix}\begin{bmatrix}\mathbf{V}_1^{n+1} \\ \mathbf{X}_S^{n+1}\end{bmatrix} = \\ &\begin{bmatrix}\left(\frac{\Delta z}{\Delta t}\mathbf{C} - \frac{1}{\Delta t}\mathbf{Q}_1\right) & \mathbf{0} \\ \mathbf{0} & \mathbf{1}_n\end{bmatrix}\begin{bmatrix}\mathbf{V}_1^n \\ \mathbf{X}_S^n\end{bmatrix} \\ &+ \begin{bmatrix}\left(\mathbf{P}_S + \frac{1}{\Delta t}\mathbf{Q}_S\right) \\ \Delta t\mathbf{N}_S\end{bmatrix}\mathbf{S}_S^{n+1} \\ &+ \begin{bmatrix}\mathbf{I}_S^n - \frac{1}{\Delta t}\mathbf{Q}_S\mathbf{S}_S^n - 2\mathbf{I}_1^{n+1/2} - \frac{\Delta z}{\Delta t}\mathbf{C}[\mathbf{E}_{T,1}^{n+1} - \mathbf{E}_{T,1}^n] \\ \mathbf{0}\end{bmatrix}.\end{aligned} \quad (25)$$

These simultaneous equations are solved for the new terminal voltages, $\mathbf{V}_1^{n+1}$, and state variables, $\mathbf{X}_S^{n+1}$. Vectors $\mathbf{S}_S^{n+1}$, $\mathbf{S}_S^n$, and $\mathbf{E}_{T,1}^{n+1}$, $\mathbf{E}_{T,1}^n$ contain the independent lumped sources in the termination network and the effects of the incident field, respectively, all of which are readily evaluated at the appropriate time steps. Vectors $\mathbf{V}_1^n$, $\mathbf{X}_S^n$, $\mathbf{I}_1^{n+1/2}$, and $\mathbf{I}_S^n$ are evaluated at the previous time step. Similarly, discretizing and combining (19b) and (22) yields the recursion relations for the load termination network as shown in (26), at the bottom of the page. All variables in the right-hand side of (26) are known.

In the case of resistive terminations, the state-variable characterizations of (21) and (22) become

$$\mathbf{I}_S = -\mathbf{G}_S\mathbf{V}_1 + \mathbf{G}_S\mathbf{V}_S \quad (27a)$$

$$\mathbf{I}_L = -\mathbf{G}_L\mathbf{V}_{\mathrm{NDZ}+1} + \mathbf{G}_L\mathbf{V}_L. \quad (27b)$$

Hence $\mathbf{X}_S = \mathbf{X}_L = 0$ so that $\mathbf{M}_S = \mathbf{N}_1 = \mathbf{N}_S = \mathbf{O}_S = \mathbf{Q}_1 = \mathbf{Q}_S = 0$ and $\mathbf{M}_L = \mathbf{N}_{\mathrm{NDZ}+1} = \mathbf{N}_L = \mathbf{O}_L = \mathbf{Q}_{\mathrm{NDZ}+1} = \mathbf{Q}_L = 0$ and $\mathbf{P}_1 = -\mathbf{G}_S$, $\mathbf{P}_S = \mathbf{G}_S$, $\mathbf{P}_{\mathrm{NDZ}+1} = -\mathbf{G}_L$, $\mathbf{P}_L = \mathbf{G}_L$. Equations (25) and (26) reduce to

$$\begin{aligned}&\left(\frac{\Delta z}{\Delta t}\mathbf{C} + \mathbf{G}_S\right)\mathbf{V}_1^{n+1} \\ &= \left(\frac{\Delta z}{\Delta t}\mathbf{C} - \mathbf{G}_S\right)\mathbf{V}_1^n - 2\mathbf{I}_1^{n+1/2} + \mathbf{G}_S(\mathbf{V}_S^{n+1} + \mathbf{V}_S^n) \\ &\quad - \frac{\Delta z}{\Delta t}\mathbf{C}[\mathbf{E}_{T,1}^{n+1} - \mathbf{E}_{T,1}^n]\end{aligned} \quad (28a)$$

and

$$\begin{aligned}&\left(\frac{\Delta z}{\Delta t}\mathbf{C} + \mathbf{G}_L\right)\mathbf{V}_{\mathrm{NDZ}+1}^{n+1} \\ &= \left(\frac{\Delta z}{\Delta t}\mathbf{C} - \mathbf{G}_L\right)\mathbf{V}_{\mathrm{NDZ}+1}^n - 2\mathbf{I}_{\mathrm{NDZ}+1}^{n+1/2} \\ &\quad + \mathbf{G}_L(\mathbf{V}_L^{n+1} + \mathbf{V}_L^n) \\ &\quad - \frac{\Delta z}{\Delta t}\mathbf{C}[\mathbf{E}_{T,\mathrm{NDZ}+1}^{n+1} - \mathbf{E}_{T,\mathrm{NDZ}+1}^n]\end{aligned} \quad (28b)$$

which are identical to those derived in [1] for this special case.

The solution sequence is as follows. First write the state-variable descriptions of the terminations as given in (21) and (22). Equations (25) and (26) are then solved for the line voltages, $\mathbf{V}_1^{n+1}$ and $\mathbf{V}_{\mathrm{NDZ}+1}^{n+1}$, and state variables of the termination networks, $\mathbf{X}_S^{n+1}$ and $\mathbf{X}_L^{n+1}$. Next the line voltages, $\mathbf{V}_k^{n+1}$ for $k = 2, \cdots,$ NDZ are obtained from (16b). Finally, the currents are updated for $k = 1, \cdots,$ NDZ via (16a) as

$$\begin{aligned}&\mathbf{I}_k^{n+3/2} = \\ &\mathbf{F}^{-1}\left(\frac{\Delta z}{\Delta t}\mathbf{L} - \frac{\Delta z}{2}\mathbf{A} + \frac{\Delta z}{\sqrt{\pi\Delta t}}Z_0(0)\mathbf{B}\right)\mathbf{I}_k^{n+1/2} \\ &- \frac{\Delta z}{\sqrt{\pi}\sqrt{\Delta t}}\mathbf{F}^{-1}\mathbf{B}\sum_{m=1}^{n} Z_0(m)\,[\mathbf{I}_k^{n+3/2-m} - \mathbf{I}_k^{n+1/2-m}] \\ &- \mathbf{F}^{-1}(\mathbf{V}_{k+1}^{n+1} - \mathbf{V}_k^{n+1}) \\ &- \mathbf{F}^{-1}\left\{[\mathbf{E}_{T,k+1}^{n+1} - \mathbf{E}_{T,k}^{n+1}] - \frac{\Delta z}{2}[\mathbf{E}_{L,k}^{n+3/2} + \mathbf{E}_{L,k}^{n+1/2}]\right\}\end{aligned} \quad (29a)$$

$$\begin{aligned}&\begin{bmatrix}\left(\frac{\Delta z}{\Delta t}\mathbf{C} - \mathbf{P}_{\mathrm{NDZ}+1} - \frac{1}{\Delta t}\mathbf{Q}_{\mathrm{NDZ}+1}\right) & -\mathbf{O}_L \\ -\Delta t\mathbf{N}_{\mathrm{NDZ}+1} & \mathbf{1}_n - \Delta t\mathbf{M}_L\end{bmatrix}\begin{bmatrix}\mathbf{V}_{\mathrm{NDZ}+1}^{n+1} \\ \mathbf{X}_L^{n+1}\end{bmatrix} = \\ &\begin{bmatrix}\left(\frac{\Delta z}{\Delta t}\mathbf{C} - \frac{1}{\Delta t}\mathbf{Q}_{\mathrm{NDZ}+1}\right) & \mathbf{0} \\ \mathbf{0} & \mathbf{1}_n\end{bmatrix}\begin{bmatrix}\mathbf{V}_{\mathrm{NDZ}+1}^n \\ \mathbf{X}_L^n\end{bmatrix} \\ &+ \begin{bmatrix}\left(\mathbf{P}_L + \frac{1}{\Delta t}\mathbf{Q}_L\right) \\ \Delta t\mathbf{N}_L\end{bmatrix}\mathbf{S}_L^{n+1} + \begin{bmatrix}\mathbf{I}_L^n - \frac{1}{\Delta t}\mathbf{Q}_L\mathbf{S}_L^n - 2\mathbf{I}_{\mathrm{NDZ}+1}^{n+1/2} - \frac{\Delta z}{\Delta t}\mathbf{C}[\mathbf{E}_{T,\mathrm{NDZ}+1}^{n+1} - \mathbf{E}_{T,\mathrm{NDZ}+1}^n] \\ \mathbf{0}\end{bmatrix}.\end{aligned} \quad (26)$$

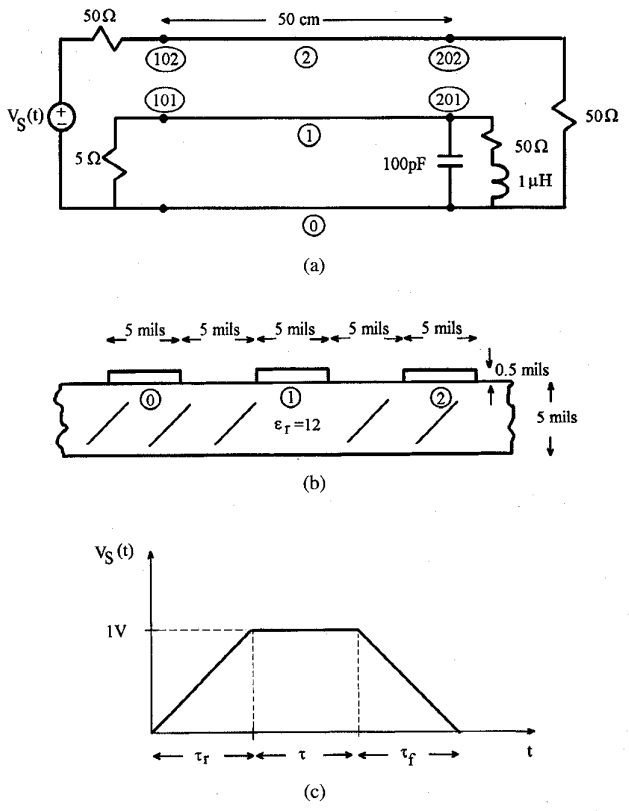

Fig. 4. The PCB used in the computation, (a) terminal constraints, (b) cross section, and (c) the source waveform.

where

$$\mathbf{F}^{-1} = \left[\frac{\Delta z}{\Delta t}\mathbf{L} + \frac{\Delta z}{2}\mathbf{A} + \frac{\Delta z}{\sqrt{\pi \Delta t}} Z_0(0)\mathbf{B}\right]^{-1}. \tag{29b}$$

The right-hand side of (29a) is multiplied by a minus sign for k = NDZ in accordance with Fig. 3. The convolution term in (29a) can be conveniently and efficiently evaluated via the Prony method as in [1], [2]. It is known [2] that for the lossless, single velocity case, a necessary condition for the stability of the solution requires that the temporal and spatial discretizations should satisfy the Courant condition which is $\Delta t \leq \Delta z/v_p$ where v_p is the phase velocity of the medium. We will assume that the similar condition applies to the multimode, multivelocity MTL case where v_p is the maximum of the phase velocities of the modes along the line.

We will assume that the Δt remains constant throughout the solution in which case the coefficient matrices of (25) and (26) are constant and need be inverted only once at the beginning of the solution. The number of state variables for a network is less than the number of required variables for a MNA analysis, and hence the dimensions of the above coefficient matrices are smaller than those of [5]. In addition, the method of [5] requires the allotment of one-half cell of the line in the termination networks, thereby further increasing the size of those associated coefficient matrices. The method of [5] also neglects the skin-effect loss of the conductors and uses only the dc resistance. The skin effect loss affects the early-time response so that for fast risetime signals, neglecting the skin effect loss may incur substantial error, as will be shown in the computed results to be presented. This method implements the backward Euler method at all stages, whereas the method of [5] requires that the backward Euler implementation be relaxed in order to provide an explicit update equation.

The first-order, backward Euler, or Adams–Moulton method used to discretize the state-variable equations is absolutely stable regardless of time step size [10]. However, it gives first-order accuracy. This would seem to degrade the second-order accuracy inherent in the FDTD discretization. However, the following results will show that the accuracy of the overall results is not substantially degraded. Excellent results can be obtained with the maximum spatial and temporal step size, as is the case for resistive terminations. It is also possible to use a second-order accurate Adams–Moulton algorithm which is also absolutely stable regardless of step size [10]. Both Adams–Moulton algorithms handle stiff systems (those with widely separated eigenvalues or time constants) well. The second-order Adams–Moulton algorithm when used to discretize the state-variable equations gives

$$\begin{aligned}\mathbf{X}_S^{n+1} &= \mathbf{X}_S^n + \frac{\Delta t}{2}\mathbf{M}_S[\mathbf{X}_S^{n+1} + \mathbf{X}_S^n] \\ &\quad + \frac{\Delta t}{2}\mathbf{N}_1[\mathbf{V}_1^{n+1} + \mathbf{V}_1^n] \\ &\quad + \frac{\Delta t}{2}\mathbf{N}_S[\mathbf{S}_S^{n+1} + \mathbf{S}_S^n] \qquad (30a)\end{aligned}$$

$$\begin{aligned}\tfrac{1}{2}[\mathbf{I}_S^{n+1} + \mathbf{I}_S^n] &= \tfrac{1}{2}\mathbf{O}_S[\mathbf{X}_S^{n+1} + \mathbf{X}_S^n] + \tfrac{1}{2}\mathbf{P}_1[\mathbf{V}_1^{n+1} + \mathbf{V}_1^n] \\ &\quad + \tfrac{1}{2}\mathbf{P}_S[\mathbf{S}_S^{n+1} + \mathbf{S}_S^n] \\ &\quad + \frac{1}{\Delta t}\mathbf{Q}_1[\mathbf{V}_1^{n+1} - \mathbf{V}_1^{n-1}] \\ &\quad + \frac{1}{\Delta t}\mathbf{Q}_S[\mathbf{S}_S^{n+1} - \mathbf{S}_S^{n-1}]. \qquad (30b)\end{aligned}$$

The state-variable relation for the terminations at the load in (22) can be similarly discretized. The second-order discretizations in (30) can be easily combined with (19) to give implicit relations similar to those of (25) and (26). For example, the source relations in (25) become

$$\begin{aligned}&\left(\frac{\Delta z}{\Delta t}\mathbf{C} - \mathbf{P}_1 - \frac{2}{\Delta t}\mathbf{Q}_1\right)\mathbf{V}_1^{n+1} - \mathbf{O}_S\mathbf{X}_S^{n+1} \\ &\quad = \left(\frac{\Delta z}{\Delta t}\mathbf{C} + \mathbf{P}_1 - \frac{2}{\Delta t}\mathbf{Q}_1\right)\mathbf{V}_1^n - 2\mathbf{I}_1^{n+1/2} + \mathbf{I}_S^n \\ &\qquad + \left(\mathbf{P}_S + \frac{2}{\Delta t}\mathbf{Q}_S\right)\mathbf{S}_S^{n+1} + \left(\mathbf{P}_S - \frac{2}{\Delta t}\mathbf{Q}_S\right)\mathbf{S}_S^n \\ &\qquad + \mathbf{O}_S\mathbf{X}_S^n - \frac{\Delta z}{\Delta t}\mathbf{C}[\mathbf{E}_{T,1}^{n+1} - \mathbf{E}_{T,1}^n] \qquad (31a)\end{aligned}$$

$$\begin{aligned}&-\frac{\Delta t}{2}\mathbf{N}_1\mathbf{V}_1^{n+1} + \left[1_n - \frac{\Delta t}{2}\mathbf{M}_S\right]\mathbf{X}_S^{n+1} \\ &\quad = \left[1_n + \frac{\Delta t}{2}\mathbf{M}_S\right]\mathbf{X}_S^n \\ &\qquad + \frac{\Delta t}{2}\mathbf{N}_S(\mathbf{S}_S^{n+1} + \mathbf{S}_S^n) + \frac{\Delta t}{2}\mathbf{N}_S\mathbf{V}_1^n. \qquad (31b)\end{aligned}$$

We will use the first-order relations given in (25) and (26)

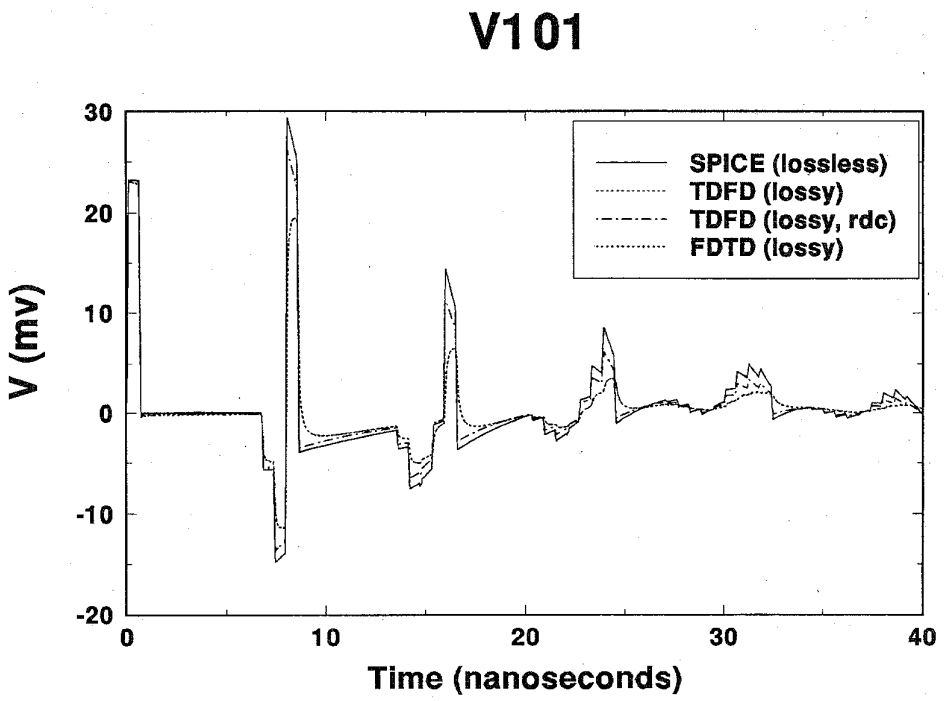

(a)

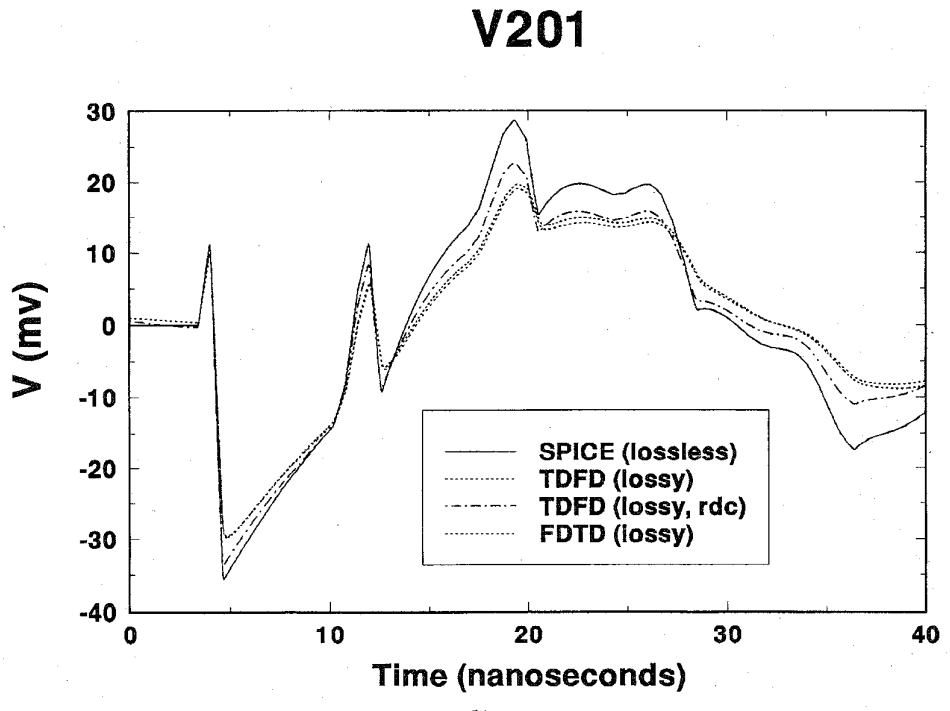

(b)

Fig. 5. Predictions of the three methods for the voltages at the terminations of the receptor line for the configuration of Fig. 4, (a) V101 and (b) V201.

since they yield simpler relations and will be shown to give adequate accuracy in the numerical results to be presented.

IV. Nonlinear Termination Networks

The above method can be similarly implemented for the case of nonlinear termination networks. The nonlinear terminations may be characterized in terms of nonlinear state-variable equations [10] as

$$\mathbf{f}(\dot{\mathbf{X}}, \mathbf{X}, \mathbf{U}, \mathbf{V}) = \mathbf{0} \tag{32a}$$

along with an associated output equation

$$\mathbf{g}(\mathbf{I}, \mathbf{X}, \mathbf{U}, \dot{\mathbf{U}}, \mathbf{V}, \dot{\mathbf{V}}) = \mathbf{0} \tag{32b}$$

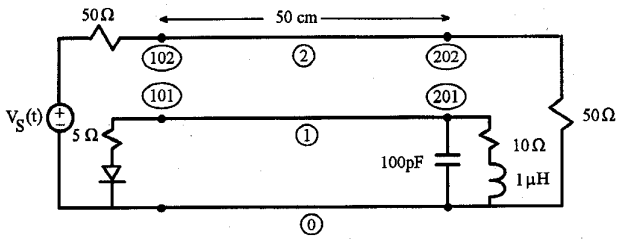

Fig. 6. The configuration of Fig. 4 with a nonlinear element (a diode).

where the dot denotes time derivative, $\mathbf{U}$ denotes the vector of independent sources in the network and $\mathbf{V}$ denotes the vector of termination voltages of the networks. The terminal update equations in (19) can be written symbolically as

$$\mathbf{h}(\mathbf{V}, \mathbf{I}) = \mathbf{0}. \tag{32c}$$

In order to solve these, we employ the predictor–corrector method [10] where the predicted value of a variable, $\mathbf{X}$, is obtained as

$$\mathbf{X}^{n+1,p} = 2\mathbf{X}^n - \mathbf{X}^{n-1} \tag{33}$$

and the corrected value of its derivative

$$\dot{\mathbf{X}}^{n+1} = \frac{1}{\Delta t}\left[\mathbf{X}^{n+1,p} - \mathbf{X}^n\right] \tag{34}$$

is substituted into (32) transforming them to a nonlinear set of algebraic equations which can be solved using, for example, the Newton–Raphson algorithm. At each time step, this solution is repeated until the error is within predetermined bounds. The remainder of the solution process continues in the same fashion as for the linear case with the updating of the interior line voltages via (16b) and the interior line currents via (29). The predictor-corrector method could also have been applied to the linear case in the previous section. However, this would complicate the relations, and we have found that sufficient accuracy can be obtained by simply solving (25) and (26) in the linear case.

V. Computed Results

To compare the predictions of these models we will investigate a three-conductor transmission line shown in Fig. 4(b). Three Copper conductors of rectangular cross section of width 5 mils (1 mil = 25.4 μm) and thickness 0.5 mils are separated by 5 mils and placed on one side of a Silicon substrate having $\varepsilon_r = 12$ and thickness 5 mils. The total line length is 50 cm and is terminated as shown in Fig. 4(a). The source is a 1 V trapezoidal pulse having a rise/fall time of $\tau_r = \tau_f = 100$ ps and pulse width of $\tau = 500$ ps. The per-unit-length inductance and capacitance matrices were computed using a numerical method giving

$$\mathbf{L} = \begin{bmatrix} 0.805756 & 0.538771 \\ 0.538\,771 & 1.077\,54 \end{bmatrix} \mu\text{H/m}$$

$$\mathbf{C} = \begin{bmatrix} 117.791 & -58.8956 \\ -58.8956 & 71.8544 \end{bmatrix} \text{pF/m}.$$

These give mode velocities in the lossless case of $v_{m1} = 1.258\,09 \times 10^8$ m/s and $v_{m2} = 1.479\,34 \times 10^8$ m/s. The per-unit-length dc resistance of each conductor is computed as $A = r_{\text{dc}} = 1/(\sigma wt) = 10.6897\,\Omega/\text{m}$. The break frequency where this transitions to the high-frequency resistance that varies as $\sqrt{f}$ is computed as the point where $wt/(w+t) = 2\delta$ giving $f_o = 131.054$ MHz [1]. The factor B is computed as

$$\begin{aligned} B &= \frac{1}{2(t+w)}\sqrt{\frac{\mu}{\sigma}} \\ &= \frac{r_{\text{dc}}}{\sqrt{\pi f_o}} \\ &= 5.268\,24 \times 10^{-4}. \end{aligned}$$

The state-variable characterizations of the source and load given in (21) and (22) become

$$\begin{aligned} \mathbf{M}_S &= \mathbf{0}, \\ \mathbf{N}_1 &= \mathbf{0}, \\ \mathbf{N}_S &= \mathbf{0}, \\ \mathbf{O}_S &= \mathbf{0}, \\ \mathbf{P}_1 &= \begin{bmatrix} -\dfrac{1}{R_{\text{NE}}} & 0 \\ 0 & -\dfrac{1}{R_S} \end{bmatrix}, \\ \mathbf{P}_S &= \begin{bmatrix} 0 \\ \dfrac{1}{R_S} \end{bmatrix}, \\ \mathbf{Q}_1 &= \mathbf{0}, \\ \mathbf{Q}_S &= \mathbf{0} \end{aligned}$$

and

$$\begin{aligned} \mathbf{M}_L &= \begin{bmatrix} -\dfrac{R}{L} \end{bmatrix}, \\ \mathbf{N}_{\text{NDZ+1}} &= \begin{bmatrix} \dfrac{1}{L} & 0 \end{bmatrix}, \\ \mathbf{N}_L &= \mathbf{0}, \\ \mathbf{O}_L &= \begin{bmatrix} -1 \\ 0 \end{bmatrix}, \\ \mathbf{P}_{\text{NDZ+1}} &= \begin{bmatrix} 0 & 0 \\ 0 & -\dfrac{1}{R_L} \end{bmatrix}, \\ \mathbf{P}_L &= \mathbf{0}, \\ \mathbf{Q}_{\text{NDZ+1}} &= \begin{bmatrix} -C & 0 \\ 0 & 0 \end{bmatrix}, \\ \mathbf{Q}_L &= \mathbf{0} \end{aligned}$$

where $C = 100$ pF, $L = 1\,\mu$H, $R = 10\,\Omega$, $R_S = 50\,\Omega$, $R_L = 50\,\Omega$, and $R_{\text{NE}} = 5\,\Omega$. Observe that the capacitor produces a voltage source-capacitor loop with $[\mathbf{V}_{\text{NDZ+1}}]_1$. Hence, the derivative of $\mathbf{V}_{\text{NDZ+1}}$ in the terminal state-variable relation in (22b), $\mathbf{Q}_{\text{NDZ+1}}$, is nonzero.

We will compare the predictions of the SPICE (lossless) predictions [1], the time-domain to frequency-domain transformation (TDFD) [1], and the finite difference-time domain (FDTD) predictions of this paper. The time-domain to frequency-domain transformation modeled the source as a 10 MHz periodic trapezoidal waveform with 50% duty cycle and rise/fall times of 100 ps. In applying the TDFD method, the spectral content of the waveform to be predicted is the primary determinant of the number of harmonics required for

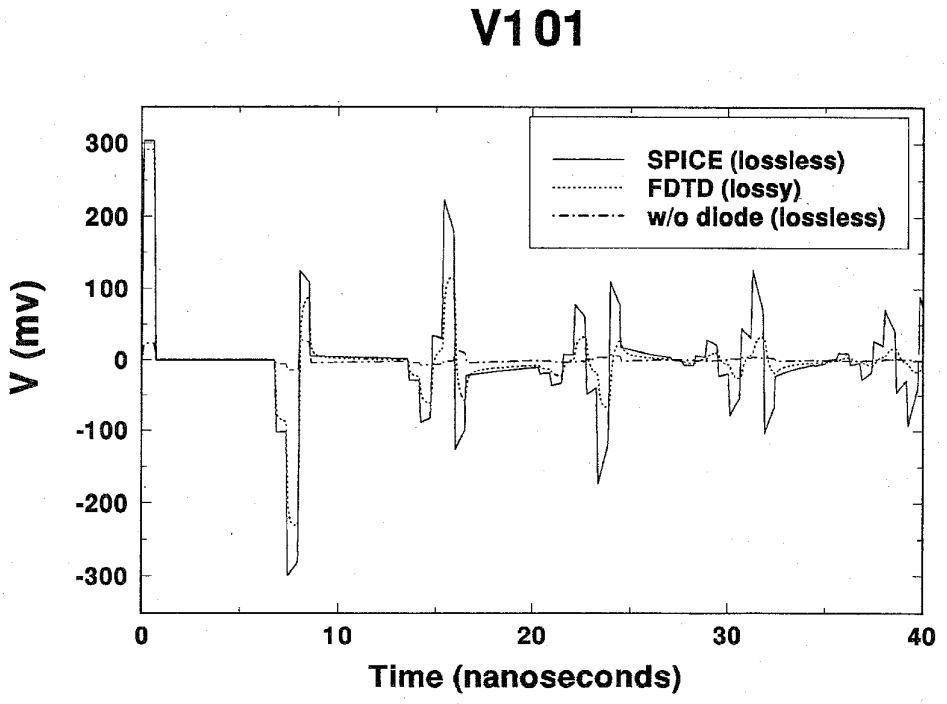

(a)

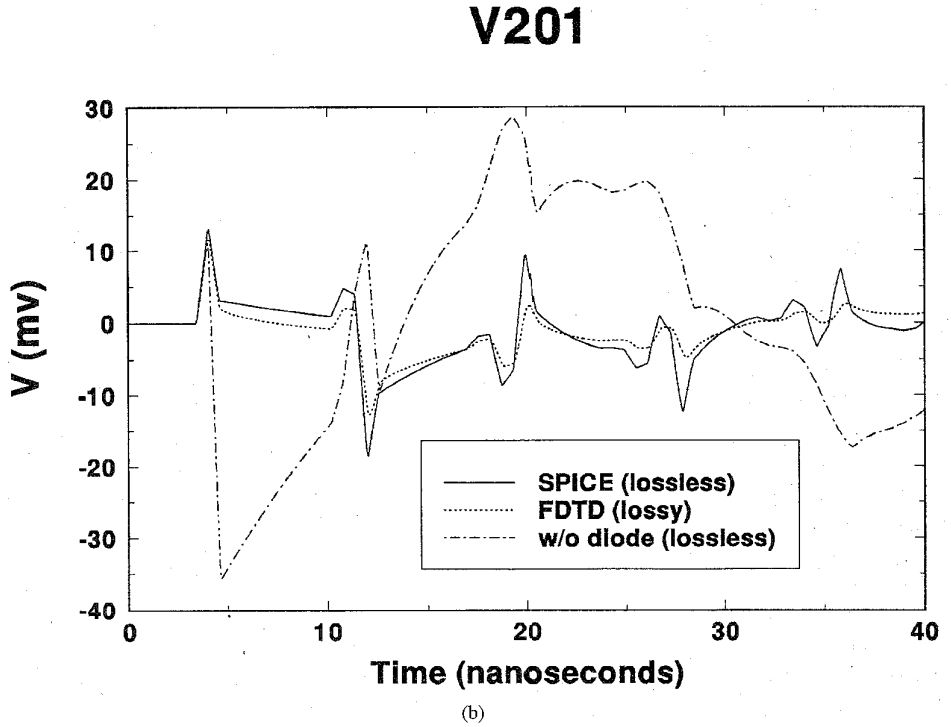

(b)

Fig. 7. Predictions of the three methods for the voltages at the terminations of the receptor line for the configuration of Fig. 6, (a) V101 and (b) V201.

an adequate characterization of the time-domain response. For the problem, the rise times of the output waveforms are on the order of 100 ps which has a spectral content extending to on the order of 10 GHz. Hence, 2000 harmonics were used in the computation of the frequency response. The FDTD spatial and temporal discretizations are denoted by

$$\mathrm{NDZ} = \frac{\mathcal{L}}{\Delta z}$$

$$\mathrm{NDT} = \frac{\text{Final Solution Time}}{\Delta t}.$$

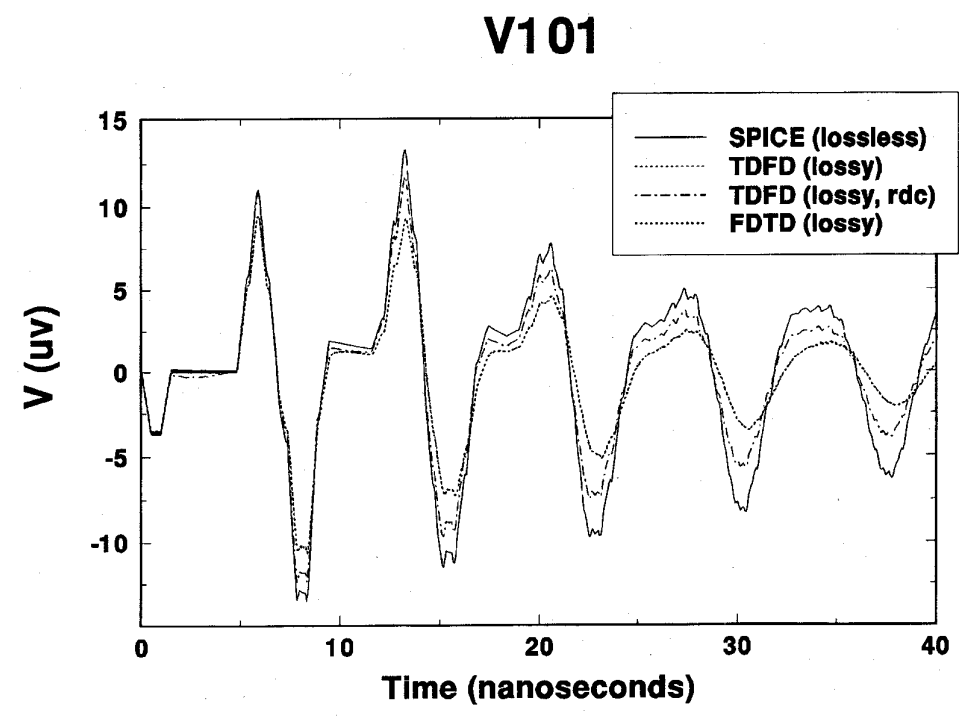

(a)

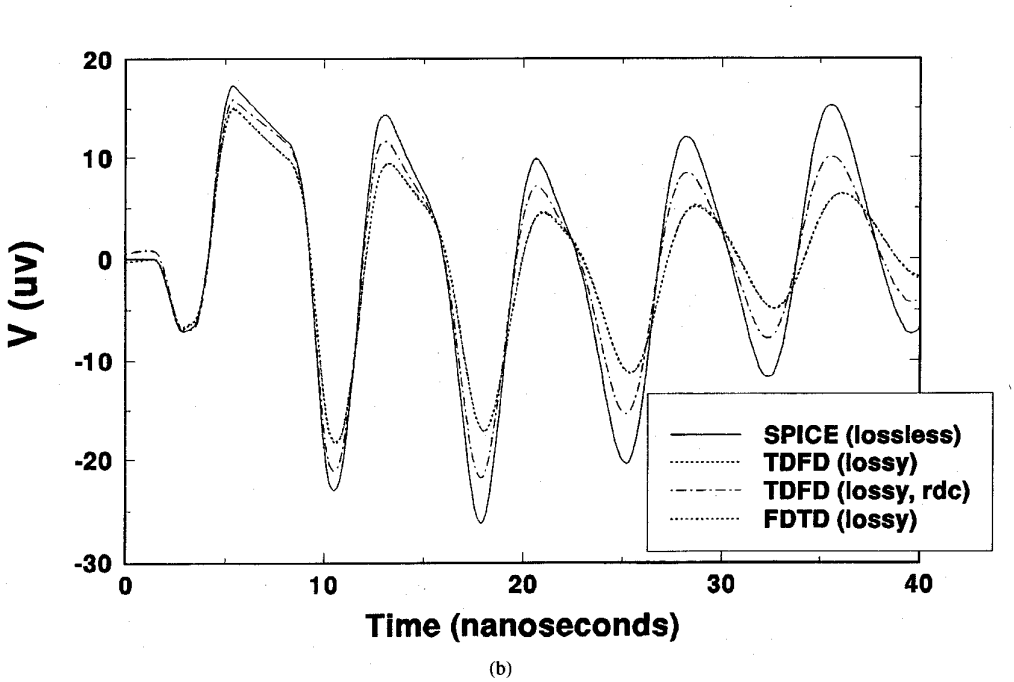

(b)

Fig. 8. Predictions of the three methods for the induced voltages across the terminations of the receptor line of Fig. 4 for incident field excitation. The incident field is a 1 V/m uniform plane wave incident along the line axis at 60° from the vertical with the electric field vector parallel to the board; (a) V101 and (b) V201.

Thus the Courant stability criterion translates to

$$\text{NDT} \geq \text{NDZ} \times (\text{Final Solution Time}) \times \frac{v}{\mathcal{L}}.$$

The spatial discretization for the FDTD results was chosen so that each cell was $\lambda/10$ using the smaller of the mode velocities, v_{m1}, at 20 GHz, giving NDZ = 795. At the Courant limit of $\Delta t = \Delta z/v$ for this spatial discretization using the larger of the mode velocities, v_{m2}, and a total solution time of 40 ns we obtain a total number of time points of NDT = 9410.

Fig. 5(a) and (b) show the predictions for voltages across the ends of the receptor line. Losses are clearly important in providing accurate predictions. In addition we have shown the predictions using only the dc resistances of the conductors, i.e., neglecting the skin effect $\sqrt{f}$ losses. This also shows that for this case the skin effect losses are significant, which is not surprising since these become important above $f_o = 131.054$ MHz and there is significant spectral content above this frequency. The FDTD predictions with this method (lossy) are virtually identical to the TDFD (lossy) results. The FDTD predictions using this method and neglecting losses were also compared to the SPICE predictions and gave identical results as they should.

Next, we consider the case of a nonlinear termination. This is obtained by inserting a diode in series with the $5\,\Omega$ load at the left end of the receptor line as shown in Fig. 6. The diode is characterized by $i_D = I_S(e^{v_D/V_T} - 1)$ where $I_S = 10$ nA and $V_T = 25$ mV. Fig. 7(a) and (b) show the corresponding predictions of the voltages across the terminations of the receptor line. Because the load is nonlinear, the TDFD model cannot be used. However, the FDTD (lossy) model indicates that losses are again important. The results without the diode (Fig. 5) are also shown to indicate the significant impact the diode has on these results. The terminal voltages without the diode are significantly smaller in V101 than with the diode present, whereas in V201, the reverse is true. Again, the FDTD predictions using this method and neglecting losses were also compared to the SPICE predictions and gave identical results as they should.

Next, we show the predictions for an incident uniform plane wave illuminating the line. The wave is incident along the line axis at a angle of 60° to the vertical axis that is normal to the board with the electric field intensity vector parallel to the board. The waveform for the electric field is a trapezoidal pulse shown in Fig. 4(c) but with a rise time of $\tau_r = \tau_f = 500$ ps and pulse width of $\tau = 500$ ps. The electric field waveform has a maximum of 1 V/m. Fig. 8 shows the resulting induced termination voltages of the receptor line. Again, the TDFD and FDTD models give virtually the same results and losses are clearly significant. The predictions using only the dc resistances of the conductors again show that skin effect losses are important for this problem. Although not shown, the FDTD predictions using this method and neglecting losses were also compared to the SPICE predictions and gave identical results as they should.

VI. Conclusions

We have presented a FDTD solution for a MTL having arbitrary terminations as well as an incident field. The state-variable representation of the terminations gives an optimal description in terms of number of unknowns and can represent general termination networks. A stable and accurate method of incorporating the terminal constraints into the FDTD recursion relation was given and shown to yield accurate predictions for the minimum Courant time step. Hence, the computational overhead for this method is minimized. The effect of skin effect losses was shown to be important. Hence, using only dc losses can result in significant prediction errors. However, the method presented easily handles these $\sqrt{f}$ type dependencies. The model is readily adapted to interconnections of transmission lines (transmission line networks), which represents the practical representation of transmission lines and will be detailed in a subsequent publication.

Acknowledgment

The authors wish to thank Dr. S. D. Gedney of the Department of Electrical Engineering, University of Kentucky, for his numerous helpful discussions.

References

[1] C. R. Paul, *Analysis of Multiconductor Transmission Lines.* NY: Wiley Interscience, 1994.
[2] K. S. Kunz and R. J. Luebbers, *The Finite Difference Time Domain Method in Electromagnetics.* Boca Raton, FL: CRC Press, 1993.
[3] A. K. Agrawal, H. J. Price, and S. H. Gurbaxani, "Transient response of multiconductor transmission lines excited by a nonuniform electromagnetic field," *IEEE Trans. Electromag. Compat.*, vol. EMC-22, pp. 119–129, May 1980.
[4] E. S. M. Mok and G. I. Costache, "Skin-effect considerations in transient response of a transmission line excited by an electromagnetic pulse," *IEEE Trans. Electromag. Compat.*, vol. 34, pp. 320–329, Aug. 1992.
[5] D. Mardare and J. LoVetri, "The finite-difference time-domain solution of lossy MTL networks with nonlinear junctions," *IEEE Trans. Electromag. Compat.*, vol. 37, pp. 252–259, May 1995.
[6] N. S. Nahman and D. R. Holt, "Transient analysis of coaxial cables using the skin effect approximation $A + B\sqrt{s}$," *IEEE Trans. Circuit Theory*, vol. 19, pp. 443–451, Sept. 1972.
[7] F. M. Tesche, "On the inclusion of losses in time-domain solutions of electromagnetic interaction problems," *IEEE Trans. Electromag. Compat.*, vol. 32, pp. 1–4, Feb. 1990.
[8] R. V. Churchill, *Operational Mathematics*, 2nd ed. NY: McGraw-Hill, 1958.
[9] C. R. Paul, "Incorporation of terminal constraints in the FDTD analysis of transmission lines," *IEEE Trans. Electromag. Compat.*, vol. 36, pp. 85–91, May 1994.
[10] L. O. Chua and P.-M. Lin, *Computer Aided Analysis of Electronic Circuits: Algorithms and Computational Techniques.* Englewood Cliffs, NJ: Prentice-Hall, 1975.
[11] B. J. Leon, *Lumped Systems.* NY: Holt, Rinehart, and Winston, 1968.

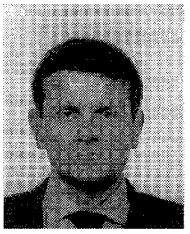

Antonio Orlandi (M'90) was born in Milan, Italy, on September 16, 1963. He received the degree in electrical engineering in 1988 from the University of Rome.

He was with the Department of Electrical Engineering of the University of Rome from 1988 to 1990. In 1990, he was appointed Assistant Professor at the Electrical Engineering Department of the University of L'Aquila, Italy. He has published papers in the fields of electromagnetic compatibility and lighting protection systems. Current research interests include numerical method to approach very fast transients characterization techniques.

Dr. Orlandi is an Associate Editor of the IEEE TRANSACTIONS ON ELECTROMAGNETIC COMPATIBILITY. He is also a member of the IEEE EMCS TC-9 Committee.

Clayton R. Paul (S'61–M'70–SM'79–F'87) was born in Macon, GA on September 6, 1941. He received the B.S. degree from the Citadel, Charleston, SC, in 1963, the M.S. degree from Georgia Institute of Technology, Atlanta, in 1964, and the Ph.D. degree from Purdue University, Lafayette, IN, in 1970, all in electrical engineering.

He has been a member of the faculty of the Department of Electrical Engineering at the University of Kentucky since 1971 and is currently Professor of Electrical Engineering. He is the author of nine textbooks on electrical engineering subjects and has published more than 100 technical papers, the majority of which are in his primary research area of electromagnetic compatibility (EMC) of electronic systems. From 1970 to 1984, he conducted extensive research for the U.S. Air Force into modeling crosstalk in multiconductor transmission lines and printed circuit boards. From 1984 to 1990, he has served as a Consultant to the IBM Corporation in the area of product EMC design.

Dr. Paul is a member of Tau Beta Pi and Eta Kappa Nu.